Coexistence of tunable Weyl points and topological nodal lines in ternary transition-metal telluride TaIrTe_{4}

Xiaoqing Zhou, Qihang Liu, QuanSheng Wu, Tom Nummy, Haoxiang Li, Justin Griffith, Stephen Parham, Justin Waugh, Eve Emmanouilidou, Bing Shen, Oleg V. Yazyev, Ni Ni, and Daniel Dessau

Phys. Rev. B **97**, 241102 — Published 8 June 2018

DOI: 10.1103/PhysRevB.97.241102

Coexistence of Tunable Weyl Points and Topological Nodal Lines in Ternary Transition-Metal Telluride $TaIrTe_4$

Xiaoqing Zhou[1,†,*], Qihang Liu[2,†,*], QuanSheng Wu[3,4], Tom Nummy[1], Haoxiang Li[1], Justin Griffith[1], Stephen Parham[1], Justin Waugh[1], Eve Emmanouilidou[5], Bing Shen[5], Oleg V. Yazyev[3,4], Ni Ni[5], and Daniel Dessau[1]

[1]*Department of Physics, University of Colorado, Boulder, CO 80309, USA*
[2]*Department of Physics, South University of Science and Technology of China, Shenzhen 518055, China*
[3]*Institute of Physics, École Polytechnique Fédérale de Lausanne (EPFL), CH-1015 Lausanne, Switzerland*
[4]*National Centre for Computational Design and Discovery of Novel Materials MARVEL, Ecole Polytechnique Fédérale de Lausanne (EPFL), CH-1015 Lausanne, Switzerland*
[5]*Department of Physics and Astronomy and California NanoSystems Institute, University of California, Los Angeles, CA 90095, USA*
† These authors contributed to the work equally.
[*]E-mail: Xiaoqing.zhou@colorado.edu, liuqh@sustc.edu.cn

Abstract

We report a combined theoretical and experimental study on $TaIrTe_4$, a potential candidate of the minimal model of type-II Weyl semimetals. Unexpectedly, an intriguing node structure with twelve Weyl points and a pair of nodal lines protected by mirror symmetry was found by first-principle calculations. Some signatures of the complex electronic structure, such as the topologically non-trivial band crossings and topologically trivial Fermi arcs, are cross-validated by angle-resolved photoemission spectroscopy. Through external strain, the number of Weyl points can be reduced to the theoretical minimum of four, and the appearance of the nodal lines can be switched between different mirror planes in momentum space. The coexistence of switchable Weyl points and nodal lines establishes transition-metal chalcogenides as a unique test ground for topological state characterization and engineering.

Topological semimetals (SMs) has recently emerged as an active topic due to their exotic physics both in bulk and surface states [1-4], represented by Weyl fermions [1,5-18], Dirac fermions [2,19-22], nodal-lines [3,9,23-28] or even quasi-particles without analogous states in the standard model of high-energy physics [29-34]. With the explosion of discovery of these topological SMs, there arises a natural question of which material should be regarded as a prototype of a given class with simple topological features, such as Bi_2Se_3 [35] for topological insulators, Na_3Bi [22] for Dirac SMs, and $CaAs_3$ for nodal-line SM [36]. A minimal approach [18] for the Weyl SM is to find the one with the band structure as clean as possible near the Fermi level (E_F) and more importantly, with the smallest number of Weyl points. Given the complication of the magnetic structure of a time-reversal breaking Weyl SM (such as Mn_3Sn [37] and $YbMnBi_2$ [38]), the target of the "hydrogen atom" model for the Weyl SMs has been focused on the inversion-breaking SMs with the minimal number of 4 Weyl points.

Recently, the family of transition-metal chalcogenides MTe$_2$ (M = Mo, W) [6,10-12,15,16] and MM'Te$_4$ (M = Ta, Nb; M' = Ir, Rh) [9,13,14,17,39] have been predicted and experimentally identified as type-II Weyl SMs, with tilted Weyl cones appearing at boundaries between electron and hole pockets by breaking Lorentz invariance [6,40]. In WTe_2 and $MoTe_2$, the underlying Weyl points are clustered together and subject to very subtle lattice constant changes [15,16], posing difficulties to identify the number of Weyl points. Furthermore, even the benchmark signature, i.e., the Fermi arcs observed in angle-resolved photoemission spectroscopy (ARPES) could often be "fake evidences" of the Weyl points because of the existence of bulk carrier pockets at the Fermi surface [11,15]. $TaIrTe_4$ has been proposed as the minimal model of Weyl SM with only four Weyl points well-separated in k-space above E_F [13], which was supported by a few experimental reports [9,17]. However, in both works [9,17] the spectra near E_F and Γ point are relatively blurry, imposing challenges to clearly identify the subtle band crossings and novel surface states. Thus, no evidence supports that the system does not host any other gap closing points.

To tell if $TaIrTe_4$ is naturally served as the minimal model of Weyl SM, we use the combination of ARPES and first-principles calculations based on density functional theory (DFT) [41-43] to resolve the electronic structure of $TaIrTe_4$, especially focusing on the details in the center of the Brillouin zone (BZ) where high momentum-resolution is required. In contrast to the previous DFT studies [9,17], our theoretical results show that $TaIrTe_4$ hosts a unique combination of twelve Weyl points and two Dirac nodal rings in the BZ. Such coexistence of different topological features has been theoretically explored [44-47] but not experimentally confirmed before. Our high momentum-resolution ARPES measurement

by 7-eV laser harmonics successfully resolved the details close to the Γ point and found band crossings below E_F as evidence of the bulk nodal lines by comparing with our DFT results. We also found apparent surface Fermi arcs that are topologically trivial, indicating the importance of the crosscheck between both theory and experiment to confirm the topological features in type-II Weyl SMs with complex Fermi surfaces. Our observation thus rules out $TaIrTe_4$ as a minimal model of Weyl SM, but establishes it as a promising candidate for topological band engineering instead. Notably, applying strain to $TaIrTe_4$ would tune the number of the Weyl points as well as the appearance of the nodal line within different mirror planes in momentum space.

Coexistence of Weyl points and nodal lines in $TaIrTe_4$. The structure of $TaIrTe_4$ could be viewed as a cell-doubling derivative of WTe_2, with 1T'-type layer structure and Bernal AB stacking. With single crystal X-ray diffraction (Fig. 1a) we determined the structure as an orthorhombic lattice with a = 3.80 Å, b = 12.47 Å and c = 13.24 Å, which was used in our DFT calculations [48]. Transport study shows clear quantum oscillations and non-saturating magnetoresistance (Fig. 1b), the latter of which is suggested to be relevant with the existence of Weyl points [49,50]. More details of the synthesis, structural data and transport properties are shown in Supplementary Note 1 [51].

Similar to type-II Weyl SMs WTe_2 and $MoTe_2$, $TaIrTe_4$ has a non-centrosymmetric $Pmn2_1$ (No. 31) space group. This structure contains four symmetry operations: identity, mirror reflection M_x, screw axis operation $\{C_{2z}|(1/2,0,1/2)\}$, and a glide reflection operation $\mathcal{M} = \{M_y|(1/2,0,1/2)\}$ that transforms (x, y, z) in position space to $(x+a/2, -y, z+c/2)$. Therefore, $\mathcal{M}^2 = -e^{i(k_x+k_z)}$ [52], which means that in the $k_y = 0$ or π plane that is invariant under $\mathcal{M}$, each band has an eigenvalue of $\mathcal{M}$ either $ie^{i(k_x+k_z)/2}$ or $-ie^{i(k_x+k_z)/2}$. In this inversion-breaking system where every band is singly degenerate, the valence and conduction bands may cross each other along a nodal line if they possess opposite $\mathcal{M}$ eigenvalues. Similarly, M_x mirror symmetry can also support nodal-line structure within the $k_x = 0$ or π plane, in the presence of SOC.

The original goals of replacing Mo/W with Ta and Ir were 1) to realize a material with only four Weyl points; and 2) to extend the separation of Weyl points in momentum space [9,13]. However, our DFT calculations by surveying the band gap over the full BZ show (see Supplementary Note 2 for details [51]) that $TaIrTe_4$ has a more complex structure of topological band degeneracies than previously suggested. Besides the four equivalent Weyl points [W1, coordinates ±(0.199, 0.071, 0) $Å^{-1}$] located in the $k_z = 0$ plane, in agreement with the previous works [9,14,17], we found another eight equivalent type-II Weyl points closer to the Γ point [W2, coordinates ±(0.079, 0.021, 0.053) $Å^{-1}$] but off the $k_z = 0$ plane. Fig. 1c

shows the connection between one set of W1 and W2 points in the DFT band structure. W1 is located 74 meV above E_F, for which pump-probe ARPES has confirmed the existence of such unoccupied Weyl cones [9]. On the other hand, the eight W2 Weyl points are 71 meV below E_F, accessible by ARPES but having smaller k-space separation than that of W1. Interestingly, in $TaIrTe_4$ we also found two nodal lines 67 meV below E_F in the $k_y = 0$ plane in the presence of SOC. Unlike the circle-like shape in other reported nodal-line candidates [9,25,26,36,53], the nodal lines in $TaIrTe_4$ do not surround any high-symmetry points, but form two symmetric, crescent-shaped parts with respect to the Γ point in the BZ (Fig. 1d). This is caused by the large anisotropy between the in-plane x and out-of-plane z directions. As described above, the SOC-robust nodal lines in the $k_y = 0$ plane are protected by the glide reflection operator $\mathcal{M}$, with their non-trivial topology verified by the Berry phase calculations [51].

ARPES measurements of $TaIrTe_4$. Since the different of surface spectra between top and bottom surface is too subtle to distinguish by experiments (see Fig. S3 and S4 [51]), we compare our experimental results with the theoretical calculation of the top surface of $TaIrTe_4$. Fig. 2c shows the Fermi surface observed with ARPES under a synchrotron light of 20 eV photon energy. The first-order features, such as the two side pockets contributed by hole carriers, are generally consistent with the DFT calculations of the bulk band (with a Fermi energy offset of -50 meV) as shown in Fig. 2a. The four W1 Weyl points fall into these two hole pockets. The E-k dispersion along the Γ-X direction is shown in Fig. 2e, with overall features similar to those from the previous work of Haubold *et al.* [17]. Nevertheless, the spectra near E_F for both of these "conventional" synchrotron measurements [17] are too blurry to compare with DFT results. To overcome this, we performed measurements in this particular area (black frame in Fig. 2e) using 7-eV laser harmonics with markedly improved energy and momentum resolution [54] and perhaps better matrix element effect (see Supplementary Note 3 [51]). The observed spectra revealed far more details than those observed using higher photon energies (as shown in Fig. 2d and Fig. 2f). In Fig. 2d, the two side pockets at $k_x = \pm 0.199$ Å^{-1} are not visible in the Fermi map, but the spectra near the center demonstrate several sharp lines representing the Fermi surface. More importantly, the calculated W2 Weyl points as well as the nodal lines are all located in this narrow region (marked in Fig. 2d), providing a much better chance to find the evidence of these topological features. As shown in Fig. 2f, the dispersion spectra are also no longer the blob of intensity as in Fig. 2e. Specifically, we found two curved branches near the Γ point from E_F to about 40 meV below.

To verify the curved feature in Fig. 2f, we next look more closely into surface dispersion by ARPES and connect it to the calculated counterpart. The momentum-resolved local density of states (LDOS)

obtained from DFT calculations for the top [001] surface is shown in Fig. 3a (the bulk DOS is shown in Fig. S5a for comparison [51]). We first focus on the k_y = 0 cut, where both W2 Weyl points and nodal lines could be resolved. Compared with bulk state, the surface LDOS from Fig. 3a suggests that as the surface band merges into the bulk band, only the left band crossing point at k_x =0.07 Å^{-1} is clearly presented. Our ARPES observation fits the calculated surface dispersion very well (as shown in Fig. 3b), with only the bands on the left of the first crossing point of the nodal line visible. In contrast, the W2 Weyl points overlaps with the second band-crossing points, and so their signatures are likely invisible under 7-eV laser harmonics. Overall, such a good agreement between DFT and ARPES confirms that $TaIrTe_4$ is not the "hydrogen atom" model for Weyl semimetals; instead, it hosts a 0+1D combination of the nodal surface that is unprecedented among the numerous topological semimetals discovered to date.

In general, type-II Weyl SM hosts a relatively complicated Fermi surface in which some topologically trivial surface states could emerge from the bulk continuum, behaving like Fermi arcs. Such trivial Fermi arcs happen in both $MoTe_2$ and WTe_2 [10,15], and also in $TaIrTe_4$. For example, Fig. 3c and 3d show the theoretical and experimental dispersion spectra below E_F at the k_y = 0.25 Å^{-1} cut. Comparing with Fig. 3c (also see Fig. S5b for bulk state [51]), we find that the parabolic electron pocket in the bulk LDOS (Fig. S3b) is truncated in the surface LDOS (Fig. 3c), indicating that only the left part of the surface state emerges from the bulk forming a trivial Fermi arc. The ARPES spectra shown in Fig. 3d show good agreement with the theoretical prediction. Particularly notable in the spectra is a dispersion that has k_x = - 0.065 Å^{-1} and terminates at -8 meV, which resembles a half of a parabolic band and thus seems like a Fermi arc. However, from the verification by DFT calculations we conclude that this appearance is merely the result of a surface band merging into the relatively invisible bulk band at this photon energy. Thus in Weyl SMs with relatively complex Fermi surfaces, the experimentally observed Fermi arc cannot serve as the direct evidence of the existence of Weyl point or the underlying topological characters [15].

For nodal line SMs, it is predicted that a "drumhead" surface state will form along the nodal-line band crossing points. However, although the nodal lines protected by specific crystal symmetry indeed lead to a nontrivial Berry phase (e.g., π in $TaIrTe_4$), such a Berry phase is not sufficient to form a topologically protected surface state. In other words, the expected "drumhead" surface state could be adiabatically deformed into the bulk continuum without any symmetry breaking. Similar situation appears in Dirac SMs where the Fermi arcs on the surface are not topologically protected and can be continuously

deformed into the case of a topological or normal insulator [55]. Therefore, we do not expect to verify the existence of nodal lines in $TaIrTe_4$ through surface states.

Tuning the topological band degeneracies by volume change. Modifying the number of Weyl points by external "knobs", such as strain, is of practical importance as it may allow achieving a simple Fermi surface with only the minimum number of Weyl nodes, and thus could offer a clearer signature of various topological properties such as the chiral anomaly [56]. On the other hand, the nodal line robust to SOC requires specific mirror symmetries (M_x and $\mathcal{M}$) as mentioned above, and thus appears only within the k_x, k_y = 0 or π mirror plane. Therefore, the location of the nodal lines could also be tuned by changing the lattice parameters. Here we studied the topological transition of bulk $TaIrTe_4$ in regards to a volume change within the range of $\alpha = \frac{V-V_0}{V} = \pm 15\%$, where V_0 is the volume under ambient pressure. Not surprisingly, the majority of change occurs along the *c*-axis, which governs the inter-plane coupling strength. We first focus on the Weyl points. Given the C_{2z} rotational symmetry and time-reversal symmetry *T*, the combined symmetry $C_{2z}T$ transfroms (k_x, k_y, k_z) to (k_x, k_y, -k_z) and maintains the chirality of the Weyl point. Therefore, besides the ordinary W2 points with arbitrary (k_x, k_y, k_z), the Weyl points could also be pinned at k_z = 0 plane, forming W1 class, which in general cannot transform to W2 points because of the charge conversion. Within the range of α considered, there are always some W1 Weyl points within the k_z = 0 plane [14] (see Fig. 4a), but with an intriguing transformation. The "original" 4 W1 Weyl points appear to be quite robust and persist until $\alpha > 6\%$. On the other hand, at $\alpha = 6\%$, 4+4 extra W1 points 34 and 58 meV below E_F emerge elsewhere and evolve into 4 at $\alpha > 6\%$. Eight W2 Weyl points below E_F emerge at $\alpha = -12\%$, approaches the k_x-k_y plane as the volume increases, and annihilates at $\alpha = 6\%$ (see Supplementary Note 4 [51]). Therefore, relatively simple node structure with minimal number of Weyl points can be obtained with $6\% \leq \alpha \leq 15\%$.

Whereas the topology of nodal lines remains unchanged under compression, it evolves dramatically with the volume expansion, as shown in Fig. 4b. As nodal lines robust to SOC requires specific mirror symmetries (M_x and $\mathcal{M}$), they appear only within the k_x, k_y = 0 or π mirror plane. The two crescent nodal lines within the k_y = 0 plane disappear at α = 6%, while two nodal lines within the k_x = 0 plane, protected by M_x, are created. Such a nodal-line transition is unprecedented among the currently reported nodal-line SMs. It has an interesting implication for device physics as the corresponding surface state can be switched between different crystal faces. The nodal lines within the k_x = 0 plane still exist for α = 12% but disappear at α = 15%. Moreover, a new pair of nodal lines within in the $k_y = \pi$ plane appear in

both cases. In the case α = 12% and 15%, the node structure is composed by 4 Weyl points and nodal lines with energies close to E_F and energy separation between the Weyl points and nodal lines about 15 meV. Therefore, we could expect a relatively simple Fermi surface for examining either Weyl or nodal-line topological features by tuning the doping levels in the same material. The volume expansion might be achieved through intercalation chemistry [57,58], which has been widely used in transition metal chalcogenides to tune the *c*-axis lattice constant.

Furthermore, we stress that the coexistence of topological order morphology we reported here might not be limited to $TaIrTe_4$ alone. Recently, it was found [59] that the topological orders are ubiquitous among the family of MX_2 or $MM'X_4$ (M, M' = transition metals, X = S, Se or Te), the evolution of which is largely determined by the interlayer coupling, i.e. c-axis lattice constant [14]. While we made the accidental discovery of coexistence of two topological orders as well as the switching of Weyl points and nodal lines in TaIrTe4, it remains an open question whether a similar, or even a more simple and accessible topological order transformation can be discovered in others among this family, especially those with similar structures such as WTe_2. As demonstrated by this work, a definite answer can only be reached with a thorough search in the momentum space with careful and precise exploration.

In conclusion, by using the combination of ARPES measurement and DFT calculations we find that $TaIrTe_4$ possesses a complex node structure with twelve Weyl points and two crescent nodal lines in the BZ, as opposed to a minimal model of Weyl SM. The delicate entanglement between conduction and valence bands also offers possibility to tune the topology of the Weyl points and nodal lines by moderate strain. By observing topologically trivial Fermi arcs at surface, this work also highlights the importance of the cross-validation between both theory and experiment to confirm the topological features in such type-II Weyl SMs.

Acknowledgements

We acknowledge Dr. C. Fang for helpful discussions, Dr. Y. D. Chuang, Dr. J. D. Denlinger and Dr. M. Hoesch for technical assistances in ARPES, Hao Zheng and Hengdi Zhao for technical assistance in structural determination. This work was carried out with the support of Diamond Light Source beamline I05 (proposal no. SI13406). This work was supported by the U.S. Department of Energy (DOE), Office of Science, Office of Basic Energy Sciences under Award Numbers DE-FG02-03ER46066 (University of Colorado) and DE-SC0011978 (UCLA). Q. L. was supported by the National Young 1000 Talents Plan. This work used resources of the National Energy Research Scientific Computing Center. The

Advanced Light Source is supported by DOE office of Science User Facility under contract No. DE-AC02-05CH11231. QSW and OY acknowledge support by the NCCR Marvel.

References

[1] X. Wan, A. M. Turner, A. Vishwanath, and S. Y. Savrasov, Physical Review B **83**, 205101 (2011).
[2] Z. Wang, Y. Sun, X.-Q. Chen, C. Franchini, G. Xu, H. Weng, X. Dai, and Z. Fang, Physical Review B **85**, 195320 (2012).
[3] A. A. Burkov, M. D. Hook, and L. Balents, Physical Review B **84**, 235126 (2011).
[4] H. Weng, X. Dai, and Z. Fang, Journal of Physics: Condensed Matter **28**, 303001 (2016).
[5] B. Q. Lv, H. M. Weng, B. B. Fu, X. P. Wang, H. Miao, J. Ma, P. Richard, X. C. Huang, L. X. Zhao, G. F. Chen, Z. Fang, X. Dai, T. Qian, and H. Ding, Physical Review X **5**, 031013 (2015).
[6] A. A. Soluyanov, D. Gresch, Z. Wang, Q. Wu, M. Troyer, X. Dai, and B. A. Bernevig, Nature **527**, 495 (2015).
[7] H. Weng, C. Fang, Z. Fang, B. A. Bernevig, and X. Dai, Physical Review X **5**, 011029 (2015).
[8] S.-Y. Xu, I. Belopolski, N. Alidoust, M. Neupane, G. Bian, C. Zhang, R. Sankar, G. Chang, Z. Yuan, C.-C. Lee, S.-M. Huang, H. Zheng, J. Ma, D. S. Sanchez, B. Wang, A. Bansil, F. Chou, P. P. Shibayev, H. Lin, S. Jia, and M. Z. Hasan, Science **349**, 613 (2015).
[9] I. Belopolski, P. Yu, D. S. Sanchez, Y. Ishida, T.-R. Chang, S. S. Zhang, S.-Y. Xu, H. Zheng, G. Chang, G. Bian, H.-T. Jeng, T. Kondo, H. Lin, Z. Liu, S. Shin, and M. Zahid Hasan, Nature Communications **8**, 492 (2016).
[10] F. Y. Bruno, A. Tamai, Q. S. Wu, I. Cucchi, C. Barreteau, A. de la Torre, S. McKeown Walker, S. Riccò, Z. Wang, T. K. Kim, M. Hoesch, M. Shi, N. C. Plumb, E. Giannini, A. A. Soluyanov, and F. Baumberger, Physical Review B **94**, 121112 (2016).
[11] K. Deng, G. Wan, P. Deng, K. Zhang, S. Ding, E. Wang, M. Yan, H. Huang, H. Zhang, Z. Xu, J. Denlinger, A. Fedorov, H. Yang, W. Duan, H. Yao, Y. Wu, S. Fan, H. Zhang, X. Chen, and S. Zhou, Nat Phys **12**, 1105 (2016).
[12] L. Huang, T. M. McCormick, M. Ochi, Z. Zhao, M.-T. Suzuki, R. Arita, Y. Wu, D. Mou, H. Cao, J. Yan, N. Trivedi, and A. Kaminski, Nat Mater **15**, 1155 (2016).
[13] K. Koepernik, D. Kasinathan, D. V. Efremov, S. Khim, S. Borisenko, B. Büchner, and J. van den Brink, Physical Review B **93**, 201101 (2016).
[14] J. Liu, H. Wang, C. Fang, L. Fu, and X. Qian, Nano Letters **17**, 467 (2017).
[15] A. Tamai, Q. S. Wu, I. Cucchi, F. Y. Bruno, S. Riccò, T. K. Kim, M. Hoesch, C. Barreteau, E. Giannini, C. Besnard, A. A. Soluyanov, and F. Baumberger, Physical Review X **6**, 031021 (2016).
[16] Z. Wang, D. Gresch, A. A. Soluyanov, W. Xie, S. Kushwaha, X. Dai, M. Troyer, R. J. Cava, and B. A. Bernevig, Physical Review Letters **117**, 056805 (2016).
[17] E. Haubold, K. Koepernik, D. Efremov, S. Khim, A. Fedorov, Y. Kushnirenko, J. van den Brink, S. Wurmehl, B. Büchner, T. K. Kim, M. Hoesch, K. Sumida, K. Taguchi, T. Yoshikawa, A. Kimura, T. Okuda, and S. V. Borisenko, Physical Review B **95**, 241108 (2017).
[18] T. M. McCormick, I. Kimchi, and N. Trivedi, Physical Review B **95**, 075133 (2017).
[19] S. M. Young, S. Zaheer, J. C. Y. Teo, C. L. Kane, E. J. Mele, and A. M. Rappe, Physical Review Letters **108**, 140405 (2012).
[20] Z. Wang, H. Weng, Q. Wu, X. Dai, and Z. Fang, Physical Review B **88**, 125427 (2013).

[21] Z. K. Liu, J. Jiang, B. Zhou, Z. J. Wang, Y. Zhang, H. M. Weng, D. Prabhakaran, S. K. Mo, H. Peng, P. Dudin, T. Kim, M. Hoesch, Z. Fang, X. Dai, Z. X. Shen, D. L. Feng, Z. Hussain, and Y. L. Chen, Nat Mater **13**, 677 (2014).
[22] Z. K. Liu, B. Zhou, Y. Zhang, Z. J. Wang, H. M. Weng, D. Prabhakaran, S. K. Mo, Z. X. Shen, Z. Fang, X. Dai, Z. Hussain, and Y. L. Chen, Science **343**, 864 (2014).
[23] Y. Chen, Y.-M. Lu, and H.-Y. Kee, Nature Communications **6**, 6593 (2015).
[24] C. Fang, Y. Chen, H.-Y. Kee, and L. Fu, Physical Review B **92**, 081201 (2015).
[25] H. Weng, Y. Liang, Q. Xu, R. Yu, Z. Fang, X. Dai, and Y. Kawazoe, Physical Review B **92**, 045108 (2015).
[26] G. Bian, T.-R. Chang, R. Sankar, S.-Y. Xu, H. Zheng, T. Neupert, C.-K. Chiu, S.-M. Huang, G. Chang, I. Belopolski, D. S. Sanchez, M. Neupane, N. Alidoust, C. Liu, B. Wang, C.-C. Lee, H.-T. Jeng, C. Zhang, Z. Yuan, S. Jia, A. Bansil, F. Chou, H. Lin, and M. Z. Hasan, Nature Communications **7**, 10556 (2016).
[27] T. Bzdusek, Q. Wu, A. Rüegg, M. Sigrist, and A. A. Soluyanov, Nature **538**, 75 (2016).
[28] E. Emmanouilidou, B. Shen, X. Deng, T.-R. Chang, A. Shi, G. Kotliar, S.-Y. Xu, and N. Ni, Physical Review B **95**, 245113 (2017).
[29] B. Bradlyn, J. Cano, Z. Wang, M. G. Vergniory, C. Felser, R. J. Cava, and B. A. Bernevig, Science **353**, 5037 (2016).
[30] H. Weng, C. Fang, Z. Fang, and X. Dai, Physical Review B **93**, 241202 (2016).
[31] B. J. Wieder, Y. Kim, A. M. Rappe, and C. L. Kane, Physical Review Letters **116**, 186402 (2016).
[32] Z. Zhu, G. W. Winkler, Q. Wu, J. Li, and A. A. Soluyanov, Physical Review X **6**, 031003 (2016).
[33] Q. Liu and A. Zunger, Physical Review X **7**, 021019 (2017).
[34] B. Q. Lv, Z. L. Feng, Q. N. Xu, X. Gao, J. Z. Ma, L. Y. Kong, P. Richard, Y. B. Huang, V. N. Strocov, C. Fang, H. M. Weng, Y. G. Shi, T. Qian, and H. Ding, Nature **546**, 627 (2017).
[35] D. Hsieh, Y. Xia, D. Qian, L. Wray, J. H. Dil, F. Meier, J. Osterwalder, L. Patthey, J. G. Checkelsky, N. P. Ong, A. V. Fedorov, H. Lin, A. Bansil, D. Grauer, Y. S. Hor, R. J. Cava, and M. Z. Hasan, Nature **460**, 1101 (2009).
[36] Y. Quan, Z. P. Yin, and W. E. Pickett, Physical Review Letters **118**, 176402 (2017).
[37] K. Kuroda, T. Tomita, M. T. Suzuki, C. Bareille, A. A. Nugroho, P. Goswami, M. Ochi, M. Ikhlas, M. Nakayama, S. Akebi, R. Noguchi, R. Ishii, N. Inami, K. Ono, H. Kumigashira, A. Varykhalov, T. Muro, T. Koretsune, R. Arita, S. Shin, T. Kondo, and S. Nakatsuji, Nature Materials **16**, 1090 (2017).
[38] S. Borisenko, D. Evtushinsky, Q. Gibson, A. Yaresko, T. Kim, M. N. Ali, B. Buechner, M. Hoesch, and R. J. Cava, ArXiv e-prints **1507**, arXiv:1507.04847 (2015).
[39] L. Li, H.-H. Xie, J.-S. Zhao, X.-X. Liu, J.-B. Deng, X.-R. Hu, and X.-M. Tao, Physical Review B **96**, 024106 (2017).
[40] Y. Xu, F. Zhang, and C. Zhang, Physical Review Letters **115**, 265304 (2015).
[41] G. Kresse and J. Furthmüller, Computational Materials Science **6**, 15 (1996).
[42] J. P. Perdew, K. Burke, and M. Ernzerhof, Phys. Rev. Lett. **77**, 3865 (1996).
[43] G. Kresse and D. Joubert, Phys. Rev. B **59**, 1758 (1999).
[44] K.-H. Ahn, W. E. Pickett, and K. W. Lee, eprint arXiv:1803.08172, arXiv:1803.08172 (2018).
[45] H. Gao, Y. Kim, J. W. F. Venderbos, C. L. Kane, E. J. Mele, A. M. Rappe, and W. Ren, eprint arXiv:1802.04815, arXiv:1802.04815 (2018).

[46] H. Zhang, Y. Xie, Z. Zhang, C. Zhong, Y. Li, Z. Chen, and Y. Chen, The Journal of Physical Chemistry Letters **8**, 1707 (2017).
[47] J.-P. Sun, D. Zhang, and K. Chang, Physical Review B **96**, 045121 (2017).
[48] We also calculated the slightly different structure used in Refs. 9 and 16 and found similar results, as shown in Supplementary Section S2.
[49] T. Liang, Q. Gibson, M. N. Ali, M. Liu, R. J. Cava, and N. P. Ong, Nat Mater **14**, 280 (2015).
[50] S. Khim, K. Koepernik, D. V. Efremov, J. Klotz, T. Förster, J. Wosnitza, M. I. Sturza, S. Wurmehl, C. Hess, J. van den Brink, and B. Büchner, Physical Review B **94**, 165145 (2016).
[51] See Supplemental Material at http://link.aps.org/supplemental/ for Refs. [60-65] and further details concerning the experiments and calculations.
[52] M2 transforms (x, y, z) to (x+a, y, z+c), and in the presence of SOC with the anti-unitary operator T behaving as $T^2 = -1$, rotates spin by 2π, leading to a factor of -1 for a spin-1/2 system.
[53] R. Yu, H. Weng, Z. Fang, X. Dai, and X. Hu, Physical Review Letters **115**, 036807 (2015).
[54] J. D. Koralek, J. F. Douglas, N. C. Plumb, Z. Sun, A. V. Fedorov, M. M. Murnane, H. C. Kapteyn, S. T. Cundiff, Y. Aiura, K. Oka, H. Eisaki, and D. S. Dessau, Physical Review Letters **96**, 017005 (2006).
[55] M. Kargarian, M. Randeria, and Y.-M. Lu, Proceedings of the National Academy of Sciences **113**, 8648 (2016).
[56] J. Xiong, S. K. Kushwaha, T. Liang, J. W. Krizan, M. Hirschberger, W. Wang, R. J. Cava, and N. P. Ong, Science **350**, 413 (2015).
[57] F. R. Gamble, J. H. Osiecki, M. Cais, R. Pisharody, F. J. DiSalvo, and T. H. Geballe, Science **174**, 493 (1971).
[58] Y. Jung, Y. Zhou, and J. J. Cha, Inorganic Chemistry Frontiers **3**, 452 (2016).
[59] M. S. Bahramy, O. J. Clark, B. J. Yang, J. Feng, L. Bawden, J. M. Riley, I. Marković, F. Mazzola, V. Sunko, D. Biswas, S. P. Cooil, M. Jorge, J. W. Wells, M. Leandersson, T. Balasubramanian, J. Fujii, I. Vobornik, J. E. Rault, T. K. Kim, M. Hoesch, K. Okawa, M. Asakawa, T. Sasagawa, T. Eknapakul, W. Meevasana, and P. D. C. King, Nature Materials **17**, 21 (2017).
[60] P. C. Canfield and Z. Fisk, Philosophical Magazine Part B **65**, 1117 (1992).
[61] S. Khim, K. Koepernik, D. V. Efremov, J. Klotz, T. Förster, J. Wosnitza, M. I. Sturza, S. Wurmehl, C. Hess, J. van den Brink, and B. Büchner, Physical Review B **94**, 165145 (2016).
[62] I. Souza, N. Marzari, and D. Vanderbilt, Physical Review B **65**, 035109 (2001).
[63] A. A. Mostofi, J. R. Yates, G. Pizzi, Y.-S. Lee, I. Souza, D. Vanderbilt, and N. Marzari, Computer Physics Communications **185**, 2309 (2014).
[64] M. P. L. Sancho, J. M. L. Sancho, J. M. L. Sancho, and J. Rubio, Journal of Physics F: Metal Physics **15**, 851 (1985).
[65] Q. Wu, S. Zhang, H.-F. Song, M. Troyer, and A. A. Soluyanov, Computer Physics Communications **224**, 405 (2018).

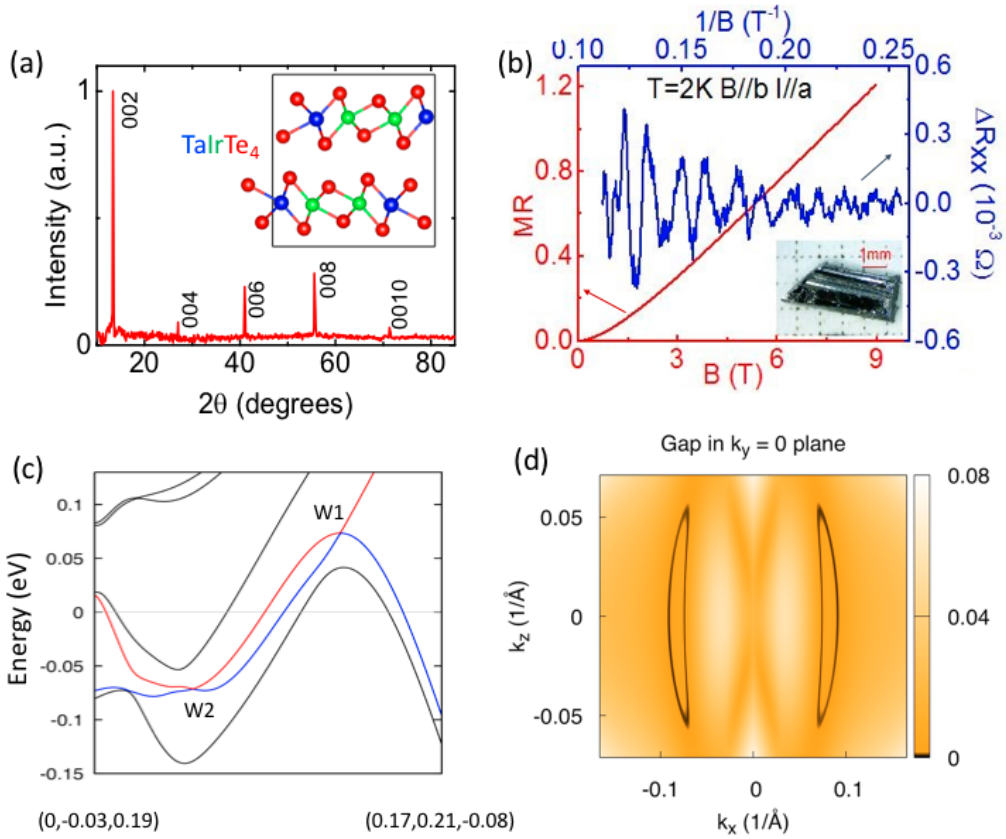

Fig. 1: (a) XRD patterns and crystal structure (inset) of $TaIrTe_4$. (b) Magnetoresistance (red) and Shubnikov-de Haas oscillations (blue). Inset: A single crystal of $TaIrTe_4$ against the 1-mm scale. (c) Band structure plotted along the path containing both W1 and W2, in the units of reciprocal lattice vectors. The red and blue lines indicate the conduction and valence band, respectively. (d) Energy gap (in units of eV) in $k_y = 0$ plane, illustrating two crescent nodal lines.

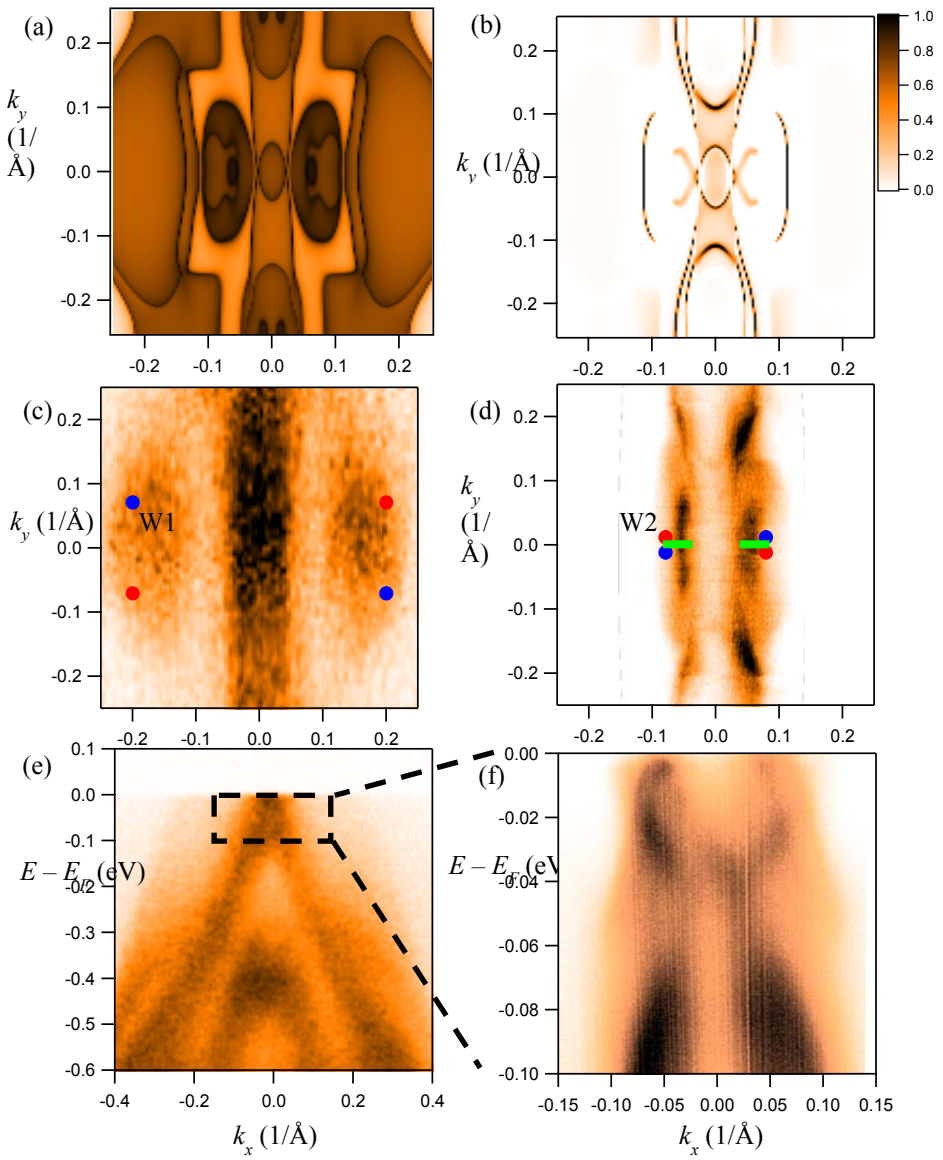

Fig. 2 (a) Momentum-resolved bulk density of states of $TaIrTe_4$ and (b) the corresponding surface-state-only counterpart calculated using DFT at energy 50 meV below E_F. (c,d) Experimental ARPES spectra of the Fermi surface taken with (c) 20-eV light, and (d) 7-eV laser harmonics. The calculated Weyl points are marked by red (Chern number +1) and blue dots (Chern number -1), whereas the nodal lines projected onto the k_x-k_y plane are represented by the green lines. (e,f) ARPES spectra along Γ-X for the (e) 28-eV light and (f) 7-eV laser harmonics respectively.

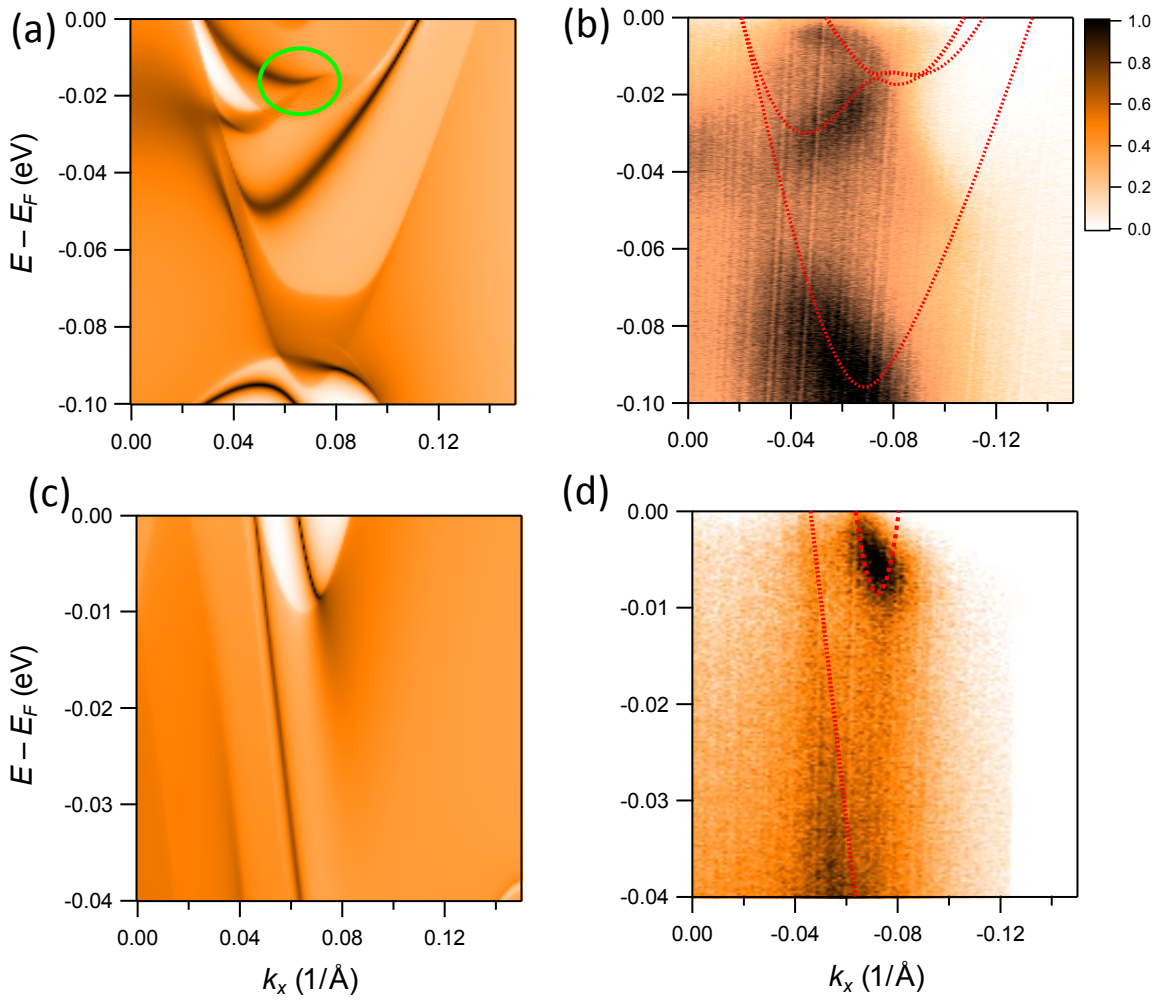

Fig. 3 (a) Momentum-resolved local density of states of $TaIrTe_4$ for the [001] surface at $k_y = 0$ obtained from DFT calculations, to be compared with (b) experimental ARPES spectra taken with 7-eV laser harmonics. (c,d) Same as (a,b) but for the cut at $k_y = 0.25$ Å^{-1}. The red dashed lines in (b) and (d) are guide-to-the-eye from DFT results.

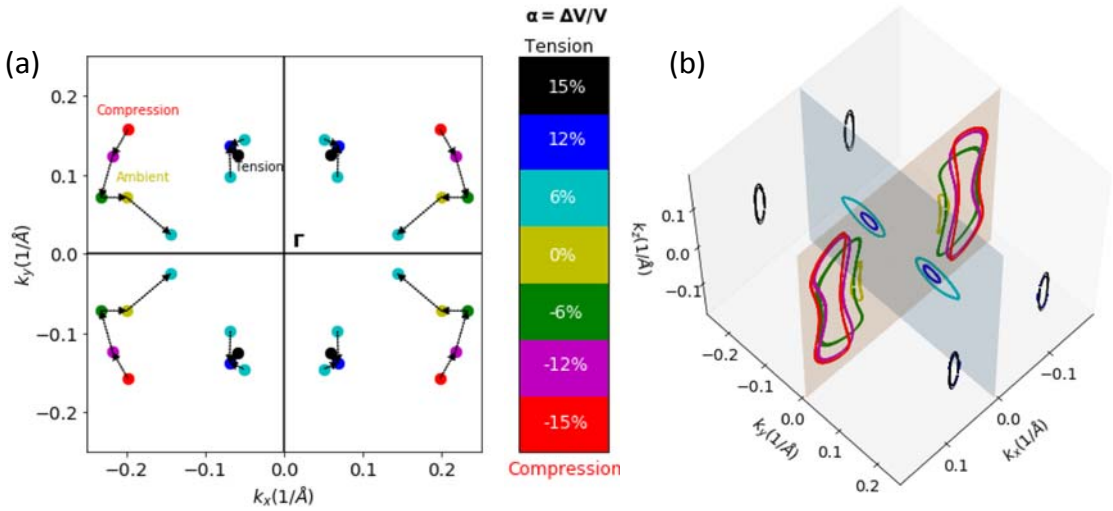

Fig. 4: (a) Evolution of Weyl points W1 upon volume change $\Delta V/V$ from -15% to 15%. (b) Nodal lines switching from the $k_y = 0$ mirror plane (red shade) to $k_x = 0$ (blue shade) and $k_y = \pi$ mirror planes with volume increase.